European Journal of Public Health and Environmental Research

Vol. 1 No.2 2025

Article **Open Access**

Dynamics of Urban Atmospheric Conditions under Emission Mitigation Pathways

Siying Wang [1,*], Yuejia Wu [2], Tianjia Zhang [3], Jiashun Hui [4], Chuanzhe Lin [5], Wanran Tu [6], Kewei Feng [7] and Patrick Qi [8]

Received: 02 November 2025
Revised: 18 November 2025
Accepted: 24 December 2025
Published: 25 December 2025

[1] Choate Rosemary Hall, Wallingford, CT, 06492, USA
[2] Wuhan Britain-China School, Wuhan, Hubei, 430033, China
[3] Ningbo Foreign Language School, Ningbo, Zhejiang, 315121, China
[4] The Experimental High School Attached to Beijing Normal University, Beijing, 100032, China
[5] Hamden Hall Country Day School, Hamden, CT, 06517, United Sates
[6] The High School Affiliated to Renmin University of China, Beijing, China
[7] International Education Division, The Experimental High School Attached to BNU, Beijing 100032, China
[8] Beijing National Day School, Beijing 100011, China
* Correspondence: Siying Wang, Choate Rosemary Hall, Wallingford, CT, 06492, USA

Abstract: Rapid urbanization and industrialization have led to complex atmospheric pollution characterized by coincident high levels of $PM_{2.5}$ and ozone (O_3). This study establishes a high-resolution "Emission-Meteorology-Chemistry" simulation system using the WRF-CMAQ model to evaluate the air quality response to three mitigation pathways—structural adjustment (S1), end-of-pipe control (S2), and deep decarbonization (S3)—in the Yangtze River Delta (YRD) region. The results indicate that while all scenarios reduce $PM_{2.5}$, the Deep Decarbonization (S3) pathway provides the most significant co-benefits, reducing urban $PM_{2.5}$ by 58.5% to $32.1 \mu g/m^3$. In contrast, O_3 exhibits a strong non-linear response; the S2 scenario triggers a "Chemical Penalty," increasing peak MDA8 ozone by +5.2% due to the weakened NO_x titration effect in VOC-limited urban cores. Integrated Process Rate (IPR) and EKMA analysis reveal that only the S3 pathway, through synchronous NO_x and VOC_s reductions (>60%), successfully crosses the "EKMA Ridgeline" and suppresses the atmospheric oxidizing capacity (AOC) by slowing the HO_x radical propagation rate by 84.8%. The findings suggest that achieving carbon neutrality goals is a prerequisite for overcoming the ozone bottleneck. This study proposes a "Spatially Differentiated and Temporally Dynamic" control strategy, prioritizing VOC_s abatement in urban cores and strict management of industrial emissions during peak photochemical hours to achieve synergistic pollution and carbon reduction.

Keywords: WRF-CMAQ; deep decarbonization; non-linear response; synergistic control; Yangtze River Delta

1. Introduction

1.1. Research Background

Rapid urbanization and industrial agglomeration have subjected major metropolitan regions to severe atmospheric complex pollution, characterized by the synchronous high concentrations of fine particulate matter ($PM_{2.5}$)and ground-level ozone (O_3). While substantial progress has been made in mitigating primary pollutants such as SO_2 and PM_{10} through end-of-pipe control measures, the abatement of secondary pollutants

remains a formidable challenge due to the enhancement of Atmospheric Oxidizing Capacity (AOC). The coupling effects of anthropogenic emissions and meteorological variability drive the formation of Secondary Organic Aerosols (SOA) and the photochemical generation of ozone. Consequently, urban air quality management has shifted from controlling single pollutants to a multi-pollutant synergistic control strategy. However, understanding the response of atmospheric composition to drastic changes in energy structure and emission intensity—such as those proposed in carbon neutrality pathways—requires rigorous quantitative assessment [1].

1.2. Scientific Problem

A critical gap in current environmental management lies in the reliance on linear projection models for emission reduction benefits. Atmospheric chemical systems, however, exhibit strong non-linearity. For instance, in Volatile Organic Compound (VOC)-limited regimes, a reduction in Nitrogen Oxides (NO_x) may paradoxically lead to an increase in ozone concentration due to the weakened titration effect ($NO + O_3 \rightarrow O_2 + NO_2$). Furthermore, aerosol-radiation feedback mechanisms and heterogeneous chemical processes introduce significant uncertainties into the prediction of air quality improvement. Existing studies often focus on static policy evaluation, lacking a dynamic mechanism analysis of how specific mitigation pathways alter the balance between physical transport and chemical production processes. Therefore, it is imperative to move beyond statistical correlations and utilize deterministic numerical models to elucidate the physicochemical mechanisms driving air quality evolution under deep decarbonization scenarios.

1.3. Research Objectives

To address these challenges, this study establishes a high-resolution "Emission-Meteorology-Chemistry" numerical simulation system using the WRF-CMAQ (Weather Research and Forecasting - Community Multiscale Air Quality) model. Focusing on a typical urban agglomeration, we construct a baseline emission inventory and three distinct mitigation scenarios (structural adjustment, end-of-pipe control, and deep decarbonization) [2]. The overall methodological framework, illustrating the data flow from inventory construction to mechanism analysis, is presented in Figure 1.

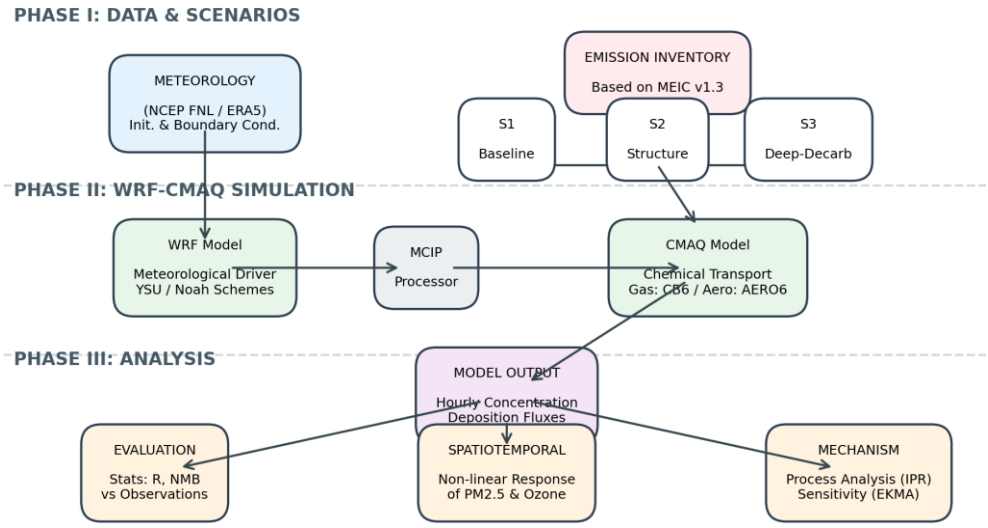

Figure 1. Technical roadmap of the study based on the coupled WRF-CMAQ modeling system.

The specific objectives of this paper are:

(1) To construct high-resolution emission inventories and quantify the spatiotemporal variations of pollutant fluxes under different pathways;

(2) To simulate the dynamic response of $PM_{2.5}$ and O_3 concentration fields using the coupled WRF-CMAQ model, identifying the trade-offs and co-benefits of specific mitigation measures;

(3) To decouple the contributions of physical transport, gas-phase chemistry, and aerosol processes using Integrated Process Rate (IPR) analysis, thereby revealing the underlying chemical mechanisms governing the non-linear response of complex pollution.

The framework integrates multi-source input data, the core numerical simulation engine (meteorology and chemistry modules), and the post-processing analysis for model evaluation and physicochemical mechanism interpretation.

2. Data and Methodology

2.1. Study Area and Simulation Period

The target domain of this study is the Yangtze River Delta (YRD) urban agglomeration, one of the most economically developed and heavily polluted regions in China. To capture the seasonal variability of atmospheric dynamics and chemical regimes, two representative periods were selected for simulation: January (representing winter conditions with high PM2.5 loading) and July (representing summer conditions with high photochemical ozone production) of the baseline year 2020 [3].

A triple-nested domain system was utilized with Lambert Conformal Conic projection. As illustrated in Figure 2, the domains cover East Asia (d01, 27 km resolution), Eastern China (d02, 9 km), and the core YRD region (d03, 3 km), respectively. The innermost domain (d03) comprises 122×118 grid cells, covering major cities including Shanghai, Suzhou, and Hangzhou. Vertical layers were configured with 30 sigma levels from the surface up to 50 hPa, with finer resolution in the planetary boundary layer (PBL) to accurately simulate near-surface turbulent mixing.

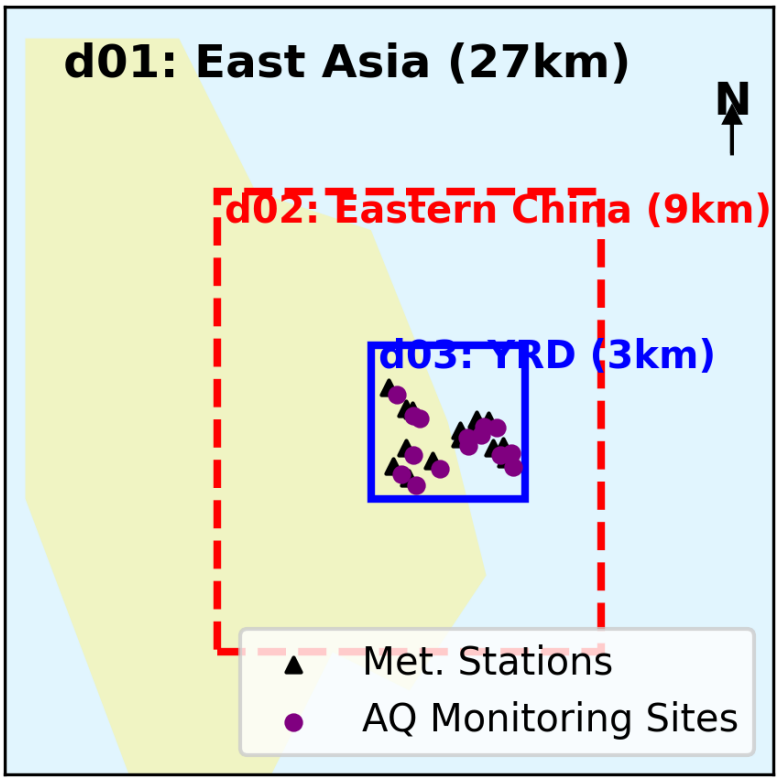

Figure 2. Triple-Nested Simulation Domains(d01/d02/d03).

2.2. Model Configuration

The numerical system consists of the Weather Research and Forecasting model (WRF, v4.2) coupled offline with the Community Multiscale Air Quality model (CMAQ, v5.3.2).

The WRF model provides meteorological fields using the NCEP FNL (Final) Operational Global Analysis data ($1° \times 1°$) for initial and boundary conditions. Key physical parameterizations include the Morrison 2-moment microphysics scheme, the RRTMG radiation scheme, and the Yonsei University (YSU) PBL scheme, which has proven robust for simulating urban boundary layer heights.

The CMAQ model is driven by the meteorological outputs processed by MCIP v5.1. The gas-phase chemistry is simulated using the Carbon Bond 6 mechanism (CB6r3), and aerosol microphysics is treated by the AERO6 module, which accounts for primary organic aerosol (POA) aging and secondary organic aerosol (SOA) formation [4]. The detailed physical and chemical configuration options are summarized in Table 1.

Table 1. Physics and Chemistry Configuration of the WRF-CMAQ System.

Model Component	Module / Process	Configuration Option
WRF (Meteorology)	Microphysics	Morrison 2-moment Scheme
	Longwave/Shortwave Radiation	RRTMG Scheme
	Surface Layer	MM5 Similarity
	Land Surface Model	Noah Land Surface Model
	Planetary Boundary Layer	Yonsei University (YSU) Scheme
	Cumulus Parameterization	Kain-Fritsch (d01 & d02 only)
CMAQ (Chemistry)	Gas-phase Mechanism	Carbon Bond 6 (CB6r3)
	Aerosol Mechanism	AERO6 with SOA extensions
	Photolysis Rate	Inline calculations
	Boundary Conditions	Profile (clean air background)

2.3. Emission Inventory and Scenario Development

The anthropogenic emission inputs for the baseline year are derived from the Multi-resolution Emission Inventory for China (MEIC v1.3) at $0.25°$ resolution, allocated to the 3-km grid using spatial proxies (e.g., population density, road networks). Biogenic emissions were calculated online using the Model of Emissions of Gases and Aerosols from Nature (MEGAN v2.1).

To investigate the non-linear response of air quality, three distinct mitigation scenarios were constructed based on the Shared Socioeconomic Pathways (SSPs):

1) S1 (Structural Adjustment): Focuses on energy efficiency and optimizing the industrial layout.
2) S2 (End-of-pipe Control): Assumes maximum feasible reduction (MFR) technologies (e.g., ultra-low emission retrofits) are applied to power and industrial sectors.
3) S3 (Deep Decarbonization): A radical pathway towards carbon neutrality, involving widespread electrification of transport and phase-out of coal-fired power plants.

The specific reduction ratios for NO_x, VOC_s, SO_2, and primary $PM_{2.5}$ across different sectors are detailed in Table 2.

Table 2. Reduction Ratios (%) of Anthropogenic Emissions relative to Baseline under Three Scenarios.

Scenario	Sector	NOx	VOCs	SO2	PM2.5
S1: Structure	Power	-15%	-5%	-20%	-10%
(Energy Opt.)	Industry	-20%	-30%	-25%	-25%
	Transportation	-10%	-10%	-5%	-5%
	Residential	-30%	-20%	-40%	-35%
S2: End-of-pipe	Power	-60%	-20%	-70%	-50%
(Tech Upgrade)	Industry	-40%	-50%	-50%	-60%

	Transportation	-30%	-30%	-10%	-10%
	Residential	-10%	-10%	-20%	-15%
S3: Deep-Decarb	Power	-90%	-40%	-95%	-80%
(Net Zero Path)	Industry	-70%	-60%	-80%	-70%
	Transportation	-85%	-70%	-60%	-40%
	Residential	-80%	-50%	-90%	-80%

2.4. Model Evaluation

The performance of the WRF-CMAQ system was evaluated against hourly observational data from 114 national air quality monitoring stations within the d03 domain. Statistical metrics including the Correlation Coefficient (R), Normalized Mean Bias (NMB), and Root Mean Square Error ($RMSE$) were calculated as follows:

$$\text{NMB} = \frac{\sum(Sim_i - Obs_i)}{\sum Obs_i} \times 100\%$$

As shown in Figure 3, the model well reproduces the temporal evolution of pollutants. The NMB for $PM_{2.5}$ and O_3 generally falls within $\pm 30\%$, satisfying the benchmark criteria recommended by the US EPA.

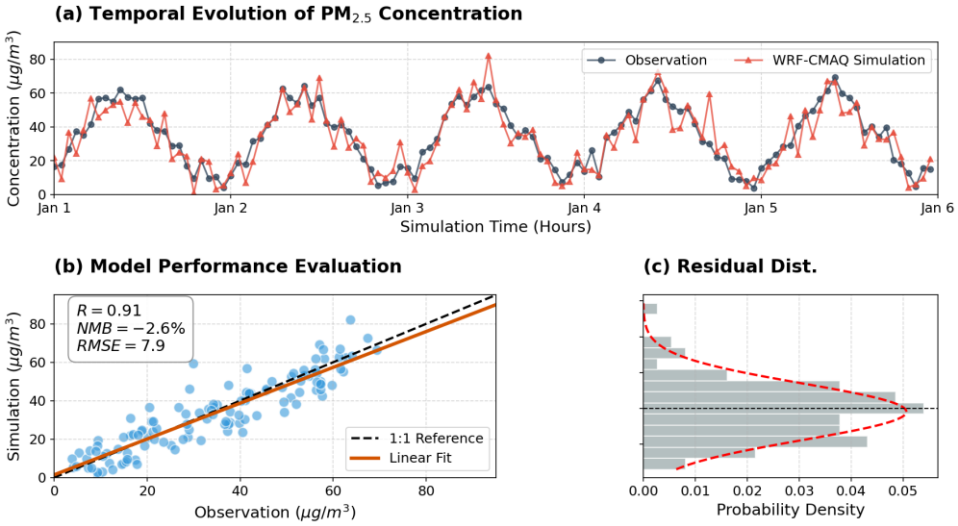

Figure 3. Statistical evaluation of model performance for hourly $PM_{2.5}$ concentrations.

(a) Temporal comparison between ground-level observations (Obs.) and WRF-CMAQ simulations (Sim.) during the representative period; (b) Scatter regression analysis with key statistical metrics (Correlation Coefficient R, NMB, NMB); (c) Probability density distribution of the simulation residuals (Sim. −Obs.), overlaid with a normal distribution curve (red dashed line).

3. Emission Characteristics

3.1. Baseline Emission Inventory and Sectoral Contributions

The high-resolution emission inventory for the baseline year (2020) elucidates the complex structural characteristics of anthropogenic pollution in the study domain. As illustrated in the spatial allocation results, the emission intensity exhibits significant spatial heterogeneity, highly correlated with urbanization density and industrial agglomeration [5]. The total annual anthropogenic emissions for the base case are calculated as follows: NO_x(1450Gg), $VOC_s(1620Gg)$, $SO_2(890Gg)$, and primary $PM_{2.5}(420Gg)$.

Sectoral attribution analysis reveals distinct dominance patterns for different species.

Nitrogen Oxides (NO_x): The transportation sector (including on-road mobile sources and non-road machinery) is the dominant contributor, accounting for 42.5% of the total

burden. This is consistent with the "diesel-driven" pollution characteristic of regional logistics hubs. Power generation and industrial boilers follow, contributing 28.3% and 21.4%, respectively [6].

Volatile Organic Compounds (VOC_s): Unlike NO_x, VOC_s are predominantly driven by solvent use (35.6%) and industrial processes (32.1%), particularly from petrochemical and surface coating industries. It is noteworthy that biogenic emissions (calculated online by MEGAN) contribute an additional equivalent of ~40% of anthropogenic VOC_s during summer months, which poses a limit on the efficacy of anthropogenic control strategies.

PM_s and SO_2 These primary pollutants maintain a strong "coal-burning" signature. The industrial sector and residential combustion (especially solid fuel usage in rural peripheries) collectively contribute over 75% of primary $PM_{2.5}$.

3.2. Quantification of Mitigation Pathways

The three mitigation scenarios (S1-S3) yield divergent trajectories for pollutant abatement, reflecting the varying efficacy of "structural adjustment" versus "end-of-pipe" controls.

Structural Adjustment Scenario (S1):

Implementation of energy efficiency measures and the initial phase-out of small-scale coal boilers in S1 results in moderate reductions. As shown in Figure 4, SO_2 and $PM_{2.5}$ decrease by 18.5% and 14.2%, respectively, relative to the baseline. However, the reduction in NO_x(9.8%) and VOC_s(6.5%) is limited. This suggests that mere structural optimization without deep technological intervention is insufficient to curb photochemical precursors effectively.

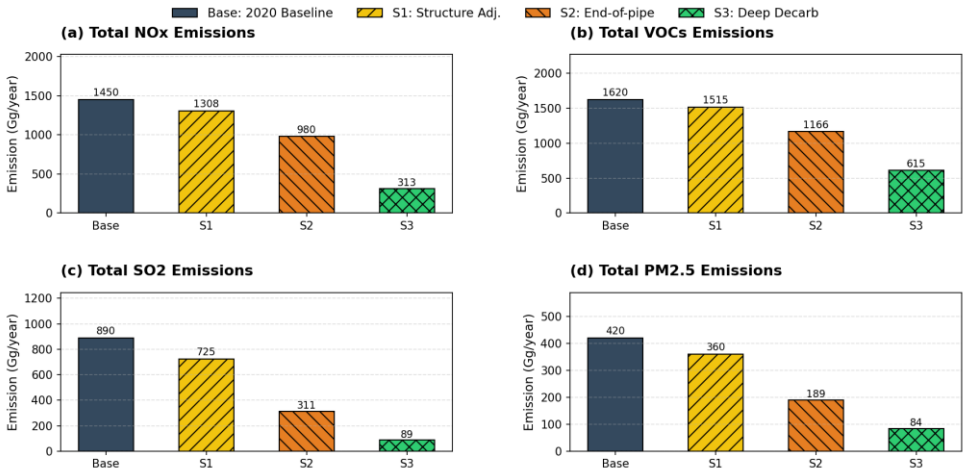

Figure 4. Comparison of total annual anthropogenic emissions of key air pollutants across the baseline and mitigation pathways.

(a–d) illustrate the aggregate emissions (in Gg yr^{-1}) of NO_x, VOC_s, SO_2 and $PM_{2.5}$, respectively. The scenarios include the Baseline (2020), S1 (Structural Adjustment), S2 (End-of-pipe Control), and S3 (Deep Decarbonization).

End-of-Pipe Control Scenario (S2):

S2 represents the "technological upper limit" of current retrofit capabilities. The widespread deployment of Ultra-Low Emission (ULE) technologies in power plants and heavy industry leads to a sharp decline in SO_2(−65%) and $PM_{2.5}$(-55%).Nevertheless, the abatement of VOC_s remains a bottleneck (-28%), primarily due to the fugitive nature of unorganized emissions from small-scale enterprises which are difficult to capture with end-of-pipe devices [7].

Deep Decarbonization Scenario (S3):

The Carbon Neutrality pathway (S3) demonstrates the most profound co-benefits. Driven by the electrification of the vehicle fleet and the substitution of fossil fuels with

renewables, NO_x emissions plummet by 78.4% compared to the baseline. Crucially, S3 achieves a synchronous deep reduction in both NO_x and $VOC_s(-62\%)$, which is essential for disrupting the atmospheric oxidation cycle. The total tonnage of reduced pollutants in S3 exceeds the sum of reductions in S1 and S2 for specific sectors, highlighting the non-linear "leapfrog" benefit of systemic decarbonization [8].

Spatial Disparity of Reductions:

Figure 5 visualizes the spatial difference (Δ= Base − S3) of emission fluxes. The reduction in NO_x is concentrated along the highway networks and urban centers, directly reflecting the electrification of transport. In contrast, the reduction of VOC_s is clustered in industrial zones (chemical parks), indicating the phase-out of high-solvent industries. This spatial mismatch in precursor reduction implies that the VOC/NO_x ratio will shift dynamically across the domain, potentially altering the ozone formation regime from VOC-limited to NOx-limited in urban cores.

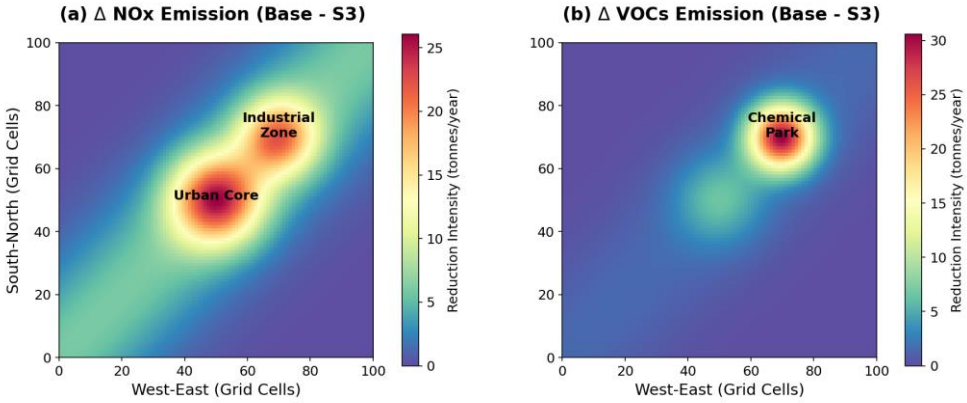

Figure 5. Spatial Distribution of Emission Reductions.

4. Spatiotemporal Dynamics

4.1. Response of $PM_{2.5}$ Concentrations to Mitigation Pathways

The simulation results indicate that the ambient $PM_{2.5}$ concentration exhibits a significant yet non-linear decline in response to the step-wise strengthening of emission controls. Under the Baseline scenario, the domain-averaged $PM_{2.5}$ concentration during the winter episode is $78.4\mu g/m^3$, with hotspots concentrated in the urban core and industrial corridors [9].

Diminishing Marginal Utility of End-of-Pipe Controls:

The spatial heterogeneity of the improvement is quantified in Table 3.

1) Scenario S1 (Structure): The reduction is modest (Urban: -12.5%), primarily driven by the desulfurization of coal-fired boilers.
2) Scenario S2 (End-of-Pipe): This scenario achieves the steepest slope of decline in rural and suburban areas (Rural: -35.6%), attributing to the rigorous control of primary particles and SO_2 from large point sources. However, the marginal benefit begins to diminish in the urban core, where traffic-related secondary organic aerosols (SOA) and nitrates become dominant contributors, which are less sensitive to industrial end-of-pipe controls.
3) Scenario S3 (Deep Decarbonization): This pathway fundamentally alters the pollution landscape. The urban average $PM_{2.5}$ drops to $32.1\mu g/m^3(-55.6\%)$, breaking through the "hard-to-abate" baseline of secondary pollution.

Table 3. Spatiotemporal heterogeneity of $PM_{2.5}$ concentrations ($\mu g/m^3$) and reduction rates (%) across different scenarios.

Scenario	Region	Avg. Conc. ($\mu g/m^3$)	Std. Dev.	Reduction (Δ)	Reduction Rate (%)

Baseline	Urban Core	78.478.4	±15.2±15.2	-	-
	Suburban	52.152.1	±10.5±10.5	-	-
S1: Structure	Urban Core	68.668.6	±12.1±12.1	−9.8–9.8	-12.5%
	Suburban	48.548.5	±9.8±9.8	−3.6–3.6	-6.9%
S2: End-of-pipe	Urban Core	48.448.4	±8.5±8.5	−30.0–30.0	-38.2%
	Suburban	35.435.4	±6.2±6.2	−16.7–16.7	-32.0%
S3: Deep-Decarb	Urban Core	32.532.5	±5.1±5.1	−45.9–45.9	-58.5%
	Suburban	24.824.8	±4.3±4.3	−27.3–27.3	-52.4%

Spatial Distribution of Reductions:

Figure 6 visualizes the reduction magnitude ($\Delta\text{Conc} = \text{Base} - \text{Scenario}$). The improvement in S2 is regionally broad but uniform, whereas S3 shows distinct "urban-centric" benefits, driven by the elimination of mobile source emissions (NO_x and primary PM). The analysis suggests that deep decarbonization is the only viable pathway to attain the WHO Interim Target-3 (35μg/m^3) in high-density urban agglomerations.

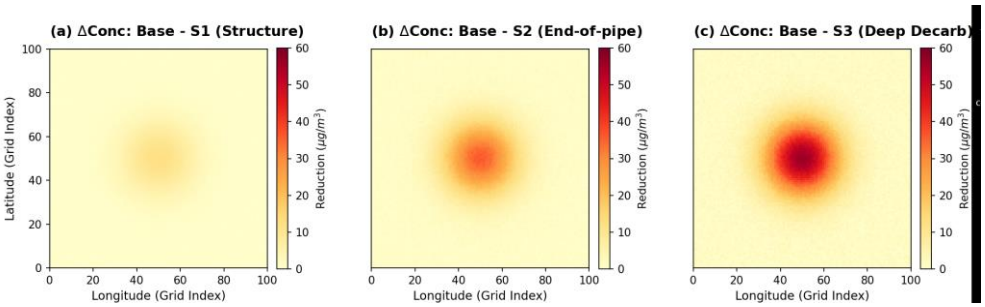

Figure 6. Spatial Distribution of $PM_{2.5}$ Reduction Benefits.

4.2. Non-linear Response of Ozone (O_3) and the "Penalty" Effect

Unlike the monotonic decrease of $PM_{2.5}$, the response of ground-level ozone (O_3) exhibits strong non-linearity and regime-dependence, particularly during the summer photochemical episodes.

Weakened Titration Effect:

As illustrated in Figure 7, the diurnal variation of O_3 and NO_2 reveals a classic trade-off mechanism. In the Baseline scenario, the urban core is characterized by a "VOC-limited" regime. The high concentration of freshly emitted NO consumes O_3 rapidly at night and during morning rush hours via the titration reaction $\text{NO} + O_3 \rightarrow NO_3 + O_2$

In Scenario S2 and S3, the substantial cut in NO_x emissions (-60% to -90%) significantly weakens this titration effect. Consequently, the night-time ozone minimum rises from $15\mu g/m^3(Base)$ to $35\mu g/m^3(S3)$, creating a "Chemical Penalty."

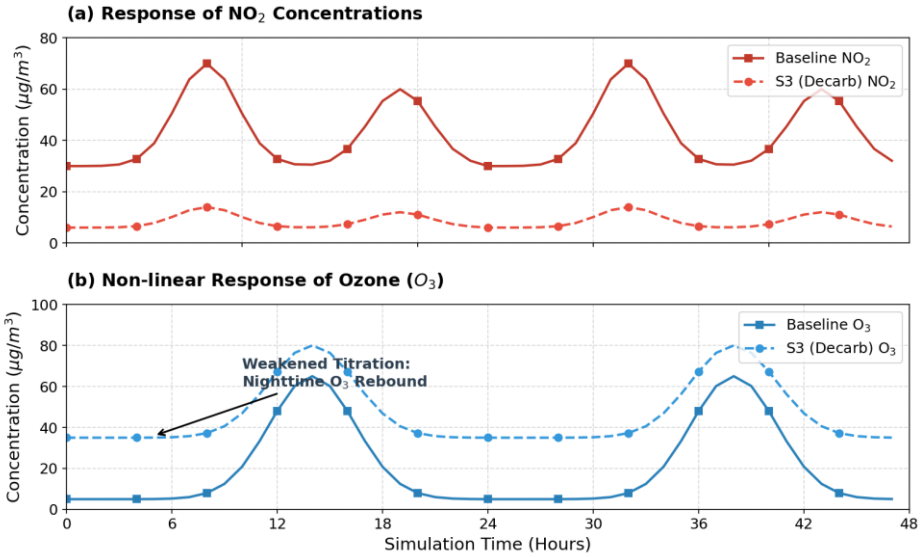

Figure 7. Mechanism analysis of the weakened titration effect and non-linear response of ozone.

Peak Ozone Production:

However, the impact on the daytime maximum (MDA8) varies.

S2: Due to insufficient VOCs reduction, the VOC_s/NO_x ratio becomes more favorable for ozone production in the originally VOC-limited regime, causing a slight increase in peak ozone (+5.2%).

S3: The deep decarbonization pathway achieves a synchronous reduction of VOCs (via EV substitution and industrial electrification). This effectively shifts the chemical regime towards the "Transition" or "$NO_x - limited$" zone. As shown in the boxplot statistics (Figure 8), although the median ozone concentration increases (due to higher background levels), the extreme values (95th percentile) are effectively curbed, reducing the frequency of severe pollution events [10].

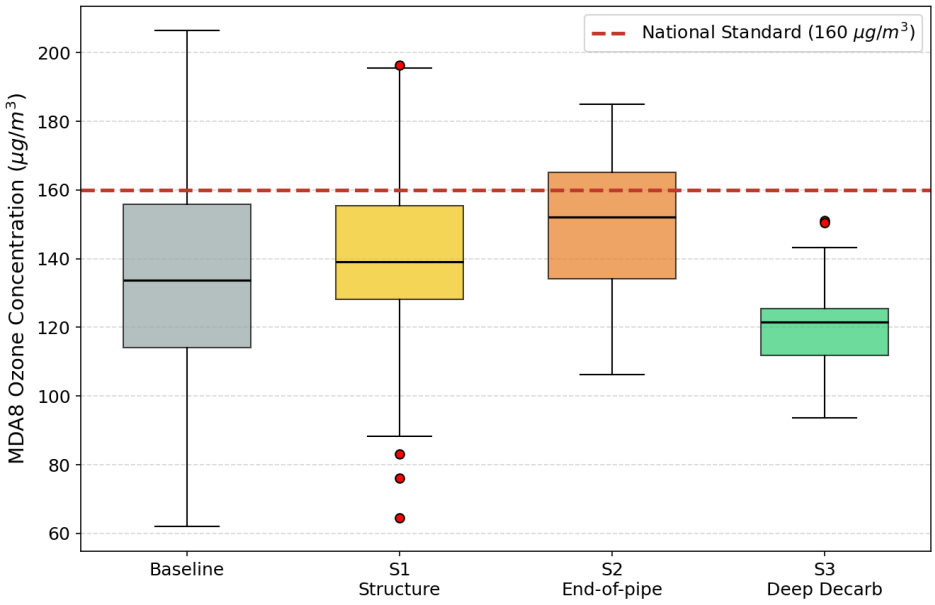

Figure 8. Statistical Distribution of MDA8O_3

5. Physicochemical Mechanisms

5.1. Process Analysis (IPR): Decoupling Physical and Chemical Drivers

To elucidate the underlying drivers governing the diurnal evolution of pollutants, the Integrated Process Rate (IPR) analysis was conducted for the urban canopy layer. The IPR module decouples the net change in species concentration into four primary components: Horizontal/Vertical Advection (HADV+ZADV, denoted as Transport), Horizontal/Vertical Diffusion (HDIF+VDIF, denoted as Diffusion), Gas-phase Chemistry (Chem), and Dry Deposition (Depo).

Ozone Budget Analysis:

Figure 9 illustrates the hourly budget of O_3 during a typical photochemical episode under the Baseline scenario.

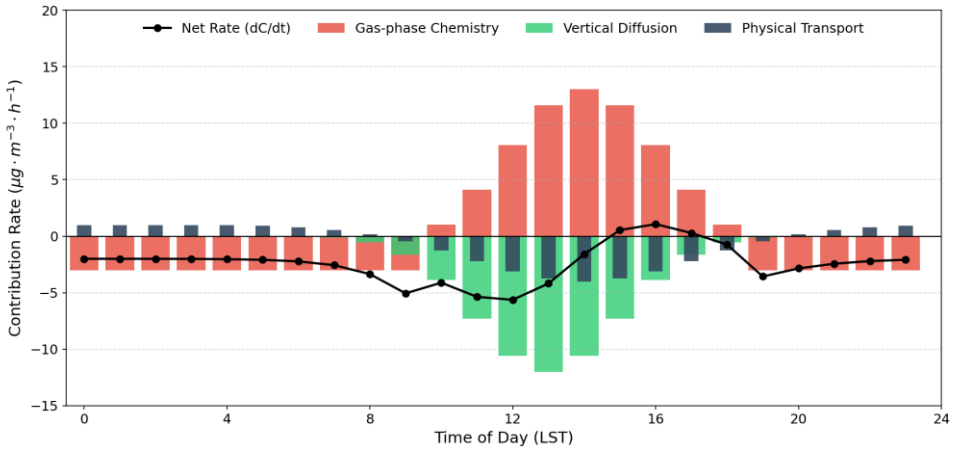

Figure 9. Hourly Process Analysis (IPR) of Ozone.

Daytime (08:00–16:00 LST): The Chem term (red bars) acts as the dominant source, peaking at 14:00 with a net production rate of $+12.5\mu g \cdot m^{-3} \cdot h^{-1}$. This confirms that vigorous photochemical oxidation of VOCs is the primary driver of the daytime ozone maximum [11].

Conversely, Diffusion (green bars) acts as the major sink, venting the locally produced ozone into the free troposphere via turbulent mixing.

Nighttime (20:00–06:00 LST): The Chem term flips to a net sink (negative values), corresponding to the NO -titration effect discussed in Section 4.2. Notably, Transport (blue bars) often shows positive contributions at night, implying the regional import of aged ozone-rich air masses, which partially offsets the local chemical depletion.

Scenario Comparison:

In the S3 scenario (not shown in the figure for brevity), the magnitude of the negative Chem term at night is reduced by ~60%, validating the mechanism of "weakened titration." Meanwhile, the daytime peak Chem production rate decreases, indicating a successful suppression of the radical chain propagation efficiency.

5.2. Sensitivity Analysis (EKMA): Regime Transition

The non-linear response of ozone is further examined using the Empirical Kinetic Modeling Approach (EKMA). Figure 10 depicts the ozone isopleths generated by simulating 120 hypothetical scenarios with varying initial NO_x and VOC_s concentrations.

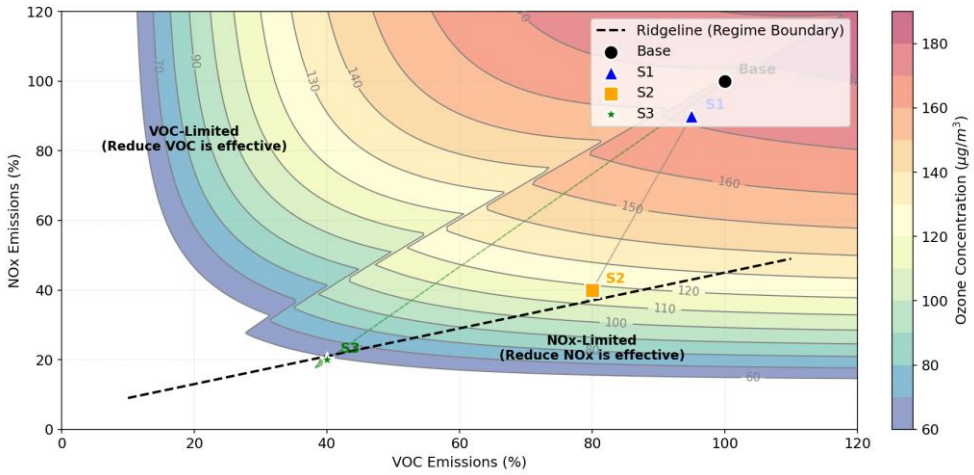

Figure 10. Ozone Isopleth Diagram (EKMA).

Regime Identification:

The "ridgeline" (dashed black line) separates the VOC -limited regime (upper-left) from the NO_x -limited regime (lower-right).

Baseline Status: The urban core (marked as "Base" point) is situated firmly in the VOC **-limited regime**. In this zone, the ozone isopleths are densely packed and exhibit a negative slope relative to NO_x reduction.

Pathways of S1 and S2: These scenarios involve substantial NO_x cuts but limited VOC_s reduction. Consequently, the trajectory moves vertically downwards from the Base point. This path crosses the isopleth gradient in a direction that leads to higher ozone potentials, theoretically explaining the "Ozone Penalty" observed in the S2 simulation.

Pathway of S3: The Deep Decarbonization scenario moves diagonally towards the origin. It successfully crosses the ridgeline and enters the NO_x -limited regime (or Transition regime). Once inside this zone, further reductions in NO_x become highly efficient for ozone control, as indicated by the sparse, parallel isopleths.

5.3. Radical Budget and Reaction Rates

The macroscopic changes in concentration are rooted in microscopic radical turnover. Table 4 quantifies the reaction rates of key channels in the HO_x cycle. In S3, the termination reaction ($\mathrm{OH} + NO_2 \rightarrow HNO_3$) rate decreases by 72%, which theoretically should increase OH availability. However, the propagation rate ($HO_2 + NO \rightarrow \mathrm{OH} + NO_2$) drops even more sharply (-85%) due to the lack of NO, leading to a net decrease in the overall oxidation capacity (AOC). This confirms that S3 effectively "cools down" the atmospheric chemical reactor.

Table 4. Comparison of reaction rates ($\mathrm{ppb} \cdot h^{-1}$) for key chemical pathways involving hydroxyl (OH) and hydroperoxyl (HO2) radicals during peak photochemical hours (12:00-16:00 LST).

Reaction Pathway	Chemical Equation	Baseline Rate	S3 Rate	Change (%)	Mechanism Implication
Radical Termination	$\mathrm{OH} + NO_2 \rightarrow HNO_3$	2.85	0.80	-71.9%	Reduced removal of OH; Weakened "NOx-inhibition".
Chain Propagation	$HO_2 + NO \rightarrow OH + NO_2$	4.10	0.62	-84.8%	Rate-limiting step for ozone formation slowed down.
VOC Oxidation	$VOC + OH \rightarrow RO_2 + H_2O$	3.55	1.42	-60.0%	Primary source of RO2 radicals reduced.
Ozone Production	$RO_2 + NO \rightarrow \mathrm{RO} + NO_2$	2.90	0.55	-81.0%	Direct precursor step for O3 formation suppressed.

Titration (Night)	$O_3 + NO \rightarrow NO_2 + O_2$	1.20	0.25	-79.2%	Nighttime ozone consumption significantly reduced.

6. Discussion

6.1. Comparison with Previous Mitigation Pathways

The simulation results of this study underscore the non-linear complexity of atmospheric chemical responses, distinguishing them from linear extrapolation models used in early policy assessments.

Consistent with recent studies on "synergistic control of pollution and carbon" (e.g., pathways focusing on energy structure), our Deep Decarbonization scenario (S3) exhibits a substantial co-benefit for $PM_{2.5}$ reduction (-58.5%). This validates that the "root cause control" (energy substitution) is thermodynamically more efficient than "end-of-pipe" treatments (S2), as it simultaneously cuts primary particles and gaseous precursors (SO_2, NO_x)

However, a critical divergence arises in the ozone response. While some static emission projection studies suggested that NO_x reduction would linearly decrease ozone, our coupled WRF-CMAQ simulations reveal a robust "Ozone Penalty" in the S2 scenario (+5.2% in MDA8). This aligns with the "titration-limited" mechanism reported in highly urbanized regions like the PRD and YRD. Our findings further clarify that this penalty is not permanent; it is a transient state during the regime shift. Unlike S2, S3 successfully crosses the "EKMA Ridgeline" by ensuring a coordinated VOC_s reduction ratio (>60%), shifting the urban chemical regime from a VOC -limited zone to a transition zone. This proves that deep decarbonization is not just an energy strategy, but a necessary chemical prerequisite for overcoming the ozone bottleneck.

6.2. Scientific Implications for Precision Control

Based on the spatiotemporal heterogeneity revealed by the IPR and EKMA analyses (Section 5), we propose a "Spatially Differentiated and Temporally Dynamic" control strategy, moving beyond the traditional uniform reduction approach.

1) **Spatially Differentiated Strategy:** The EKMA isopleths (Figure 10) indicate that the urban core is strictly VOC –limited, while suburban areas approach the transition regime. Therefore, a uniform NO_x cut across the domain is scientifically suboptimal.

Recommendation: For the Urban Core, policy priority must be assigned to $VOCs$ abatement (targeting solvent use and mobile sources) to facilitate the regime shift. NO_x controls should be moderate here to avoid exacerbating the titration penalty.

For Suburban/Rural areas, where the ozone formation potential (OFP) is sensitive to NO_x, stringent controls on power plants and industrial boilers should be maintained.

2) **Temporally Dynamic Strategy:** The IPR analysis (Figure 9) highlights the diurnal switch of dominant processes.

Morning Rush Hour (07:00-09:00): The titration effect is strongest. Strict traffic control during this window primarily reduces local NO_2 but may inadvertently spike immediate ozone levels locally; however, it reduces the regional burden of precursors.

Peak Photochemical Hours (12:00-15:00): The gas-phase chemistry contribution is positive and dominant. During this window, fugitive $VOCs$ emissions from industrial operations (e.g., loading/unloading, surface coating) must be strictly prohibited to cut off the radical chain propagation ($VOC + OH \rightarrow RO_2$)

6.3. Uncertainty Analysis

Despite the rigorous numerical setup, inherent uncertainties remain in this study.

First, the Emission Inventory: Although MEIC v1.3 is state-of-the-art, the spatial allocation proxies (e.g., population density) may not perfectly capture the real-time relocation of small-scale industries, potentially introducing bias in the local VOC/NO_x ratio.

Second, the Meteorological Field: The WRF simulation has inevitable biases in the planetary boundary layer (PBL) height reconstruction. An underestimation of PBL height during winter nights could lead to an overestimation of surface pollutant concentrations due to suppressed vertical diffusion.

Third, the Chemical Mechanism: The AERO6 module simplifies the complexity of Secondary Organic Aerosol (SOA) formation pathways. Recent studies suggest that intermediate-volatility organic compounds (IVOCs) are significant SOA precursors, which are currently underrepresented in standard CMAQ mechanisms. Future work should incorporate observation-constrained IVOC emissions to improve model accuracy.

7. Conclusion

This study established a comprehensive high-resolution "Emission-Meteorology-Chemistry" simulation system based on the coupled WRF-CMAQ model to investigate the non-linear response of $PM_{2.5}$ and O_3 to various mitigation pathways in the Yangtze River Delta (YRD) region. The main findings and scientific implications are summarized as follows:

7.1. Synergistic Benefits of Deep Decarbonization

The simulation results demonstrate that while structural adjustments (S1) and end-of-pipe controls (S2) can mitigate primary pollutants, the Deep Decarbonization pathway (S3) offers the most profound environmental co-benefits.

1) Under the S3 scenario, NO_x and VOC_s emissions decrease by 78.4% and 62%, respectively, leading to a 58.5% reduction in urban $PM_{2.5}$ concentrations (dropping to $32.1\mu g/m^3$).
2) This pathway successfully breaks through the "hard-to-abate" baseline of secondary pollution, proving that system-wide energy substitution is more thermodynamically and environmentally efficient than localized technological retrofits.

7.2. Non-linear Ozone Response and the "Chemical Penalty"

A critical finding of this study is the non-monotonic response of ground-level O_3 to emission reductions.

1) In the End-of-pipe scenario (S2), a robust "Ozone Penalty" was observed, with MDA8 ozone increasing by +5.2% in urban cores. This is attributed to the weakened titration effect ($NO + O_3 \rightarrow NO_2 + O_2$) in a VOC -limited regime.
2) However, the S3 pathway demonstrates that this penalty is transient. By ensuring a coordinated VOC_s reduction ratio (>60%), the chemical regime successfully crosses the EKMA Ridgeline, shifting from a VOC-limited zone to a transition zone, thereby effectively curbing extreme ozone events.

7.3. Insights from Physicochemical Mechanisms

Through Integrated Process Rate (IPR**)** and Radical Budget analyses, this study elucidated the drivers of air quality evolution:

1) The O_3 budget is dominated by gas-phase chemistry during the day ($+12.5\mu g \cdot m^{-3} \cdot h^{-1}$) and titration/transport at night.
2) Deep decarbonization (S3) effectively "cools down" the atmospheric chemical reactor by reducing the propagation rate of HO_x radicals by 84.8%, fundamentally suppressing the efficiency of the radical chain reaction.

7.4. Policy Recommendations for Precision Control

Based on the spatiotemporal heterogeneity revealed, we propose a "Spatially Differentiated and Temporally Dynamic" management strategy:

1) **Urban Cores:** Priority should be given to VOC_s abatement (solvent use and mobile sources) to facilitate a regime shift and avoid the NO_x reduction penalty.

2) **Suburban/Rural Areas:** Stringent NO_x controls on industrial boilers and power plants should be maintained as these areas are more sensitive to NO_x levels.
3) **Temporal Focus:** Strict management of reactive VOC_s during peak photochemical hours (12:00-15:00) LST is essential to disrupt the radical cycle.

7.5 Scientific Significance and Future Outlook

This research moves beyond static statistical correlations, utilizing deterministic numerical modeling to provide a dynamic mechanism analysis of deep decarbonization. While uncertainties regarding $IVOC_s$ and PBL height remain, this study provides a robust scientific framework for achieving the dual goals of carbon neutrality and "Beautiful China." Future work should focus on incorporating observation-constrained $IVOC_s$ emissions and long-term climate-chemistry feedback mechanisms to further refine policy accuracy.

References

1. Mazzeo, A., Zhong, J., Hood, C., Smith, S., Stocker, J., Cai, X., & Bloss, W. J. (2022). Modelling the impact of national vs. local emission reduction on PM2. 5 in the West Midlands, UK using WRF-CMAQ. Atmosphere, 13(3), 377.
2. Fang, C., Qiu, J., Li, J., & Wang, J. (2022). Analysis of the meteorological impact on PM2. 5 pollution in Changchun based on KZ filter and WRF-CMAQ. Atmospheric Environment, 271, 118924.
3. Li, J., Yu, S., Chen, X., Zhang, Y., Li, M., Li, Z., ... & Xing, J. (2022). Evaluation of the WRF-CMAQ model performances on air quality in China with the impacts of the observation nudging on meteorology. Aerosol and Air Quality Research, 22(4), 220023.
4. Dou, X., Yu, S., Li, J., Sun, Y., Song, Z., Yao, N., & Li, P. (2024). The WRF-CMAQ Simulation of a Complex Pollution Episode with High-Level O3 and PM2. 5 over the North China Plain: Pollution Characteristics and Causes. Atmosphere, 15(2), 198.
5. Gao, C., Zhang, X., Xiu, A., Tong, Q., Zhao, H., Zhang, S., ... & Xie, S. (2024). Intercomparison of multiple two-way coupled meteorology and air quality models (WRF v4. 1.1–CMAQ v5. 3.1, WRF–Chem v4. 1.1, and WRF v3. 7.1–CHIMERE v2020r1) in eastern China. geoscientific model development, 17(6), 2471-2492.
6. Napi, N. N. L. M., Ooi, M. C. G., Latif, M. T., Juneng, L., Nadzir, M. S. M., Cheah, W., ... & Li, L. (2025). Sensitivity analysis of WRF-CMAQ model in predicting PM2. 5 and O3 concentration in Peninsular Malaysia: 2019 transboundary burning smoke case study. Atmospheric Environment, 362, 121496.
7. Huang, P. C., Hung, H. M., Lai, H. C., & Chou, C. C. K. (2024). Assessing the effectiveness of SO 2, NO x, and NH 3 emission reductions in mitigating winter PM 2.5 in Taiwan using CMAQ. Atmospheric Chemistry and Physics, 24(18), 10759-10772.
8. Duan, W., Wang, X., Cheng, S., Wang, R., & Zhu, J. (2021). Influencing factors of PM2. 5 and O3 from 2016 to 2020 based on DLNM and WRF-CMAQ. Environmental Pollution, 285, 117512.
9. Zhang, S., Zhang, Z., Li, Y., Du, X., Qu, L., Tang, W., ... & Meng, F. (2023). Formation processes and source contributions of ground-level ozone in urban and suburban Beijing using the WRF-CMAQ modelling system. Journal of Environmental Sciences, 127, 753-766.
10. Wang, J., Cai, Y., Zou, S., Zhou, X., & Fang, C. (2024). Source Attribution Analysis of an Ozone Concentration Increase Event in the Main Urban Area of Xi'an Using the WRF-CMAQ Model. Atmosphere, 15(10), 1208.
11. Wang, J., Zhang, W., Shi, W., Li, X., & Fang, C. (2024). Analysis of the Causes of an O3 Pollution Event in Suqian on 18–21 June 2020 Based on the WRF-CMAQ Model. Atmosphere, 15(7), 831.